APPENDIX D

Fluid Dynamics of a High Aspect-Ratio Jet

APPENDIX D

Fluid Dynamics of a High Aspect-Ratio Jet

Scott E. Munro *
and
K. K. Ahuja
Georgia Institute of Technology
GTRI/ATASL
Atlanta, GA, 30332-0844

Abstract

Circulation control wings are a type of pneumatic high-lift device that have been extensively researched as to their aerodynamic benefits. However, there has been little research into the possible airframe noise reduction benefits of a circulation control wing. The key element of noise is the jet noise associated with the jet sheet emitted from the blowing slot. High aspect-ratio jet acoustic results (aspect-ratios from 100 to 3,000) from a related study showed that the jet noise of this type of jet was proportional to the slot height to the 3/2 power and slot width to the 1/2 power. Fluid dynamic experiments were performed in the present study on the high aspect-ratio nozzle to gain understanding of the flow characteristics in an effort to relate the acoustic results to flow parameters. Single hot-wire experiments indicated that the jet exhaust from the high aspect-ratio nozzle was similar to a 2-d turbulent jet. Two-wire space-correlation measurements were performed to attempt to find a relationship between the slot height of the jet and the length-scale of the flow noise generating turbulence structure. The turbulent eddy convection velocity was also calculated, and was found to vary with the local centerline velocity, and also as a function of the frequency of the eddy.

Nomenclature

A -- Area (typically of nozzle)
AR -- Aspect ratio
a -- Speed of sound
a_o -- Ambient speed of sound
f -- Frequency
HARN -- High aspect-ratio nozzle
h -- Slot height or rectangular nozzle height (small dimension)
L -- Characteristic length
L_{eq} -- Characteristic length for the HARN, $L_{eq} = h^{3/4}w^{1/4}$
L_x -- Length scale (streamwise direction)
L_τ -- Integral time scale
M_c -- Convection Mach number
M_t -- Jet centerline Mach number
PIV -- Particle image velocimetry
p -- pressure
Re -- Reynolds number
R_x -- Space-correlation
$R_{x\tau}$ -- Cross-correlation
w -- width of rectangular nozzle (large dimension)
V -- Velocity
  V_c -- Turbulent eddy convection velocity
  V_j -- Jet exit velocity (fully expanded)
  V_t -- Local jet centerline velocity
x -- Streamwise dimension, typically x = 0 is nozzle exit
y -- Dimension perpendicular to major axis of nozzle, y = 0 is center of nozzle
z -- Dimension along span of nozzle (parallel to major axis), z = 0 is center of nozzle
Δx -- Spacing between hot-wires in x-direction
Δy -- Spacing between hot-wires in y-direction
ρ -- density
τ -- Time shift, used for cross-correlation

Introduction

In recent years airframe noise issues have become more important to the airline industry. Thus, new and innovative ways for reducing airframe noise have been investigated. A recent study investigated the possible acoustic benefits of using a circulation control wing (CCW) as a high lift device rather than conventional flaps. [1-4]

This study found that the major contributor to airframe noise associated with a CCW configuration is the jet sheet emitted from the blowing slot. More detailed acoustic results from a high aspect-ratio nozzle (HARN) found that the level of the jet noise scaled with an equivalent length, defined as $L_{eq} = h^{3/2}w^{1/2}$. The present study is an accompanying fluid dynamic study on the same nozzle configuration. The main objective of this study was to establish a relationship between the length-scale of the flow and the nozzle geometry in an effort to relate the acoustic results to the flow. In addition, the convection velocity of the turbulent eddies was also examined.

---

* Now working for the Naval Air Warfare Center, Weapons Division, China Lake, CA 93555-6100.

APPENDIX D

Background

Although the present study dealt exclusively with fluid dynamic measurements on a high aspect-ratio jet, an accompanying study was also performed where the acoustic characteristics of the same jet were studied. References [1, 2, and 3] discuss the acoustic work. In addition, reference [3] uses results from the present study and those of reference [2] in an effort to develop a prediction scheme for the jet noise spectra of such jets. Some of the discussion in the following sections deals with jet noise issues. In the interest of brevity, the reader is referred to the references mentioned above for background on round and rectangular jet noise. Only a brief review of rectangular jet fluid dynamic characteristics is given below.

Rectangular jets, similar to round jets, are characterized by different flow regions. In general these include the core region, the transition region, and the fully mixed turbulent region.[5] The core is characterized by an unmixed region just downstream of the nozzle exit. Eventually this disappears due to the merging of the shear layers. In a round jet, this is well defined since the shear layer is axisymmetric. However, in the case of a rectangular jet the issue is somewhat clouded. If one assumes the two dimensions to be independent, there are shear layers that grow on each of the 4 edges. The two shear layers associated with the small dimension will merge at a different location downstream than the two from the large dimension. Thus, the core is typically defined as the location where the centerline velocity falls below a certain value, usually 99% of the exit velocity. Therefore, a definite length can be associated with the core. However, one must keep in mind that the shear layers are much more complex than the round jet case.

The transition region is a region of high mixing where the jet flow is still essentially considered a 2-dimensional flow. As the flow continues downstream, the mixing eventually causes the flow to become axisymmetric. This indicates the beginning of the fully mixed region. In this region, the flow has many characteristics similar to a circular jet, including the centerline velocity decay rate proportional to x^{-1} (streamwise distance).[5] The length of the core region is dependent on the jet Mach number and temperature.[5] The velocity centerline decay has also been shown to be a function of the aspect-ratio.[5]

The region where the highest levels of noise are produced in a jet is in the core region.[5] This is where the shear is very high, and the associated velocities are also at their highest. Well downstream the flow evolves into a round jet flow, however the flow velocities are much lower than the exit condition and therefore do not radiate jet noise at comparable levels to the near exit region.[5] However, as with round jets there are many theories that have been proposed. Recently, Tam et al. have investigated nozzle shapes including rectangular jets. In their studies they have limited research to low aspect-ratio nozzles. Their results indicate that rectangular jets are actually similar to round jets.[6-10] References [7-10] show Tam's fits do indeed agree well with the experimental data. This indicates that round jet noise and rectangular jet noise are actually very similar since both can be fit to one set of generic spectral curves.

As is evident by the variation in data and theories, there is still much to be investigated in the area of rectangular jet noise. The aspect-ratios considered 'high' in the above discussion are typically one or two orders of magnitude lower than the typical aspect-ratio of a CCW system. The fluid dynamic measurements presented in this paper were taken to form a complimentary set of acoustic and flow measurements on the same system in order to relate to the acoustic and fluid dynamic properties.

Objectives

It is well established that the acoustic radiation of a jet is related to the length-scales of the flow. In a round jet, the length-scale has been found to be proportional to the diameter of the jet. However, this is not as clear with a rectangular jet flow since there are two definite dimensions and the confusion is increased by the transitioning of the flow into an axisymmetric flow far downstream.

Hot-wires were used to obtain basic information about the jet flow, including: jet profiles, turbulence intensity profiles, centerline velocity, and the associated frequency spectra. Two-wire measurements were also made in the shear layer of the jet in an attempt to find the length-scales of the flow. An attempt was also made to obtain PIV (particle image velocimetry) data. However, due to the small size of the slot, detailed velocity information could not be obtained. However, the images themselves made for high quality flow visualization.

The PIV data will be presented first to give a general view of the flow. Then single hot-wire measurements will be presented to demonstrate how the jet flow is similar to other rectangular jet data and theoretical 2-dimensional jet flow calculations. Finally, space-time correlation data will be presented along with an analysis of the length-scales to determine the relationship between the geometry and the length-scales.

Fabrication of the High Aspect-Ratio Nozzle

The high aspect-ratio nozzle (HARN) was designed and built in order to obtain reliable jet noise data for high aspect-ratio rectangular jets as part of an investigation examining the acoustic characteristics of circulation control wing high lift devices. It was

designed to have variable height and width so that a wide range of aspect-ratios could be tested. Much care was taken to ensure low internal noise, thus providing a test article where pure jet noise could be studied.

The upstream portion of the HARN connects to a 4" diameter pipe flange, the standard connection in all the flow facilities at GTRI, via a round-to-rectangular duct section. The inlet of the HARN is 2.75" X 2.75" and expands from the inlet dimensions to 30" wide by 0.25" high over a streamwise distance of 30" as shown in figure 1. Knife-edge blades are attached to the HARN exit to provide the final contraction to the small nozzle heights. Shims can be placed under the blades to change the height. Blanking plates were also fabricated so that the width of the nozzle could be varied as well.

Initial experiments indicated that the top and bottom plates of the HARN deflected from the air pressure used to generate the flow. In order to minimize internal noise, tie-down rods were not used to prevent the deflection. Instead, stiffening beams were added on the outside of the structure to maintain an unobstructed flow path internal to the HARN. These beams can be seen in figure 1. More details of the HARN design and internal noise issues can be found in reference [1].

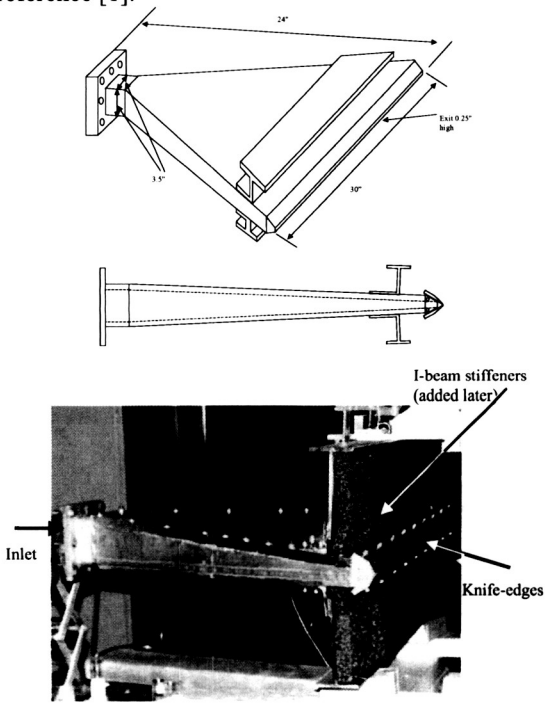

Figure 1: Harn Nozzle.

Particle Image Velocimetry Measurements

PIV Experimental Set-Up.

A PIV system is helpful in ascertaining the general instantaneous characteristics of a flow. It provides both an overall image of the flow field and the velocity vectors for an entire plane in the flow. The PIV system used for the present investigation was a TSI Incorporated two-dimensional PIV system. The system includes two lasers, a camera and software for a PC platform to run the system and acquire the data. The lasers are positioned with lenses so that the beam is turned into a laser sheet. The sheet is positioned as desired in the flow, and the camera is positioned such that the focal plane of the camera is the same plane as the laser sheet. The lasers are synchronized so that they pulse at a set time increment. Both images are recorded by the camera. The displacement of the seed particles for the two images are compared by the software, and velocity vectors are calculated. The process is all integrated into the software, from the acquisition of the images to calculation of the velocity vectors. As with most flow visualization, acquisition of quality PIV data is not trivial and is dependent on several factors that must be adjusted, including the seeding density, the image time separation, and careful positioning of the camera and lasers.

For the HARN PIV tests, the laser sheet was positioned to align with the minor axis of the jet as depicted in figure 2. This essentially provided a flow visualization 'slice' of the jet. The camera was positioned 90° to the laser sheet such that the edge of the nozzle was visible at the upstream edge of the image. The camera was focused as close as possible to try to resolve the small core of the jet. The flow was seeded with titanium-dioxide powder by using a pressurized shaker that distributed the powder into the facility plenum chamber. PIV images were taken at several jet velocities.

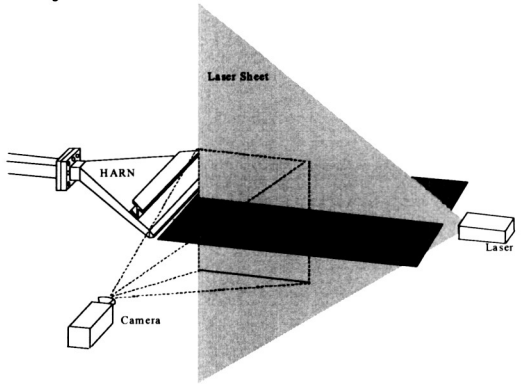

Figure 2: Schematic of PIV set-up.

PIV Analysis and discussion

The PIV system was used to acquire general flow visualization images and to extract instantaneous flow velocity vectors from the images. In general, the size of the jet was too small to adequately extract flow velocities from the core region of the jet. The lenses available with this system were not suitable for focusing in on the extremely small potential core of the jet. However, the images were able to provide spectacular flow visualization images.

The PIV experiments were performed in the High Temperature Flow Facility (HTFF) where the PIV system is routinely used. The HTFF has a high pressure air supply and an acoustically treated plenum to absorb any upstream flow and valve noise. The HARN mounts to the downstream exit of the plenum. The PIV images were recorded at several jet exit velocities, including 10 ft/s, 60 ft/s, 450 ft/s, 700 ft/s, and 850 ft/s.

Figures 3 - 6 show some typical images for four different exit velocities: 10, 60, 460, and 720 ft/s. Some of the images' contrast and brightness were changed to make the jet visible. This does not change the content of the image, however it does brighten the background of the image revealing details that might not be visible in another image that did not need to be altered to view the jet. Also, at the higher speeds the flow could not be seeded as well as at the low speeds. This limits the detail of the image and its appearance for visual comparison from one velocity to the next. One must therefore exercise caution in drawing conclusions from one image to the next. For example, after examining figure 4 one might conclude that the jet is actually not as wide as the jet in figure 5. However, hot-wire data indicate that this is not the case and that in fact the two jets have very similar spreading characteristics.

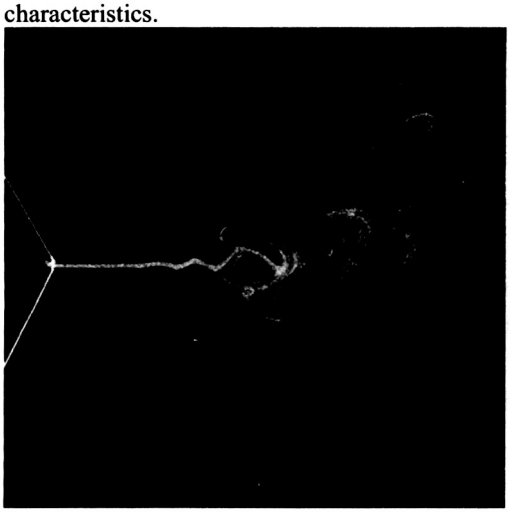

Figure 3: Sample PIV image, Vj = 10 ft/s.

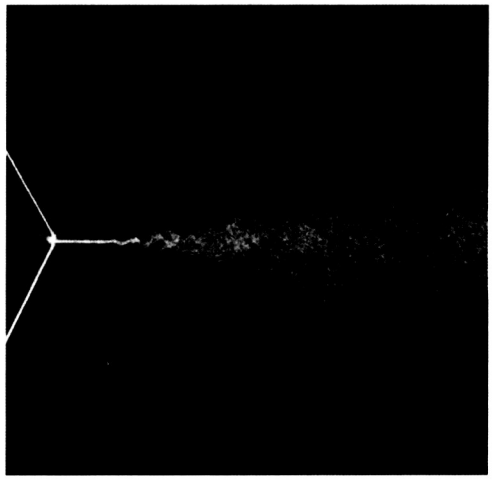

Figure 4: Sample PIV image, Vj = 60 ft/s.

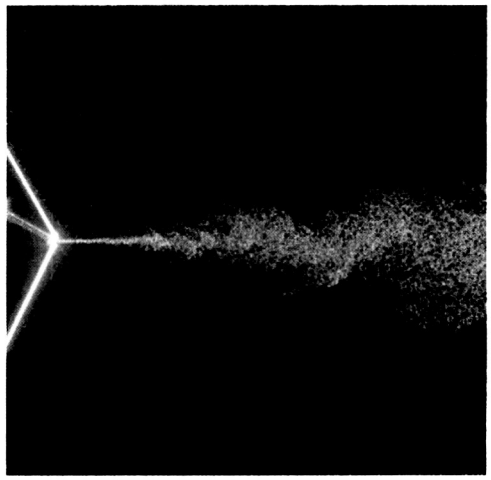

Figure 5: Sample PIV image, Vj = 460 ft/s.

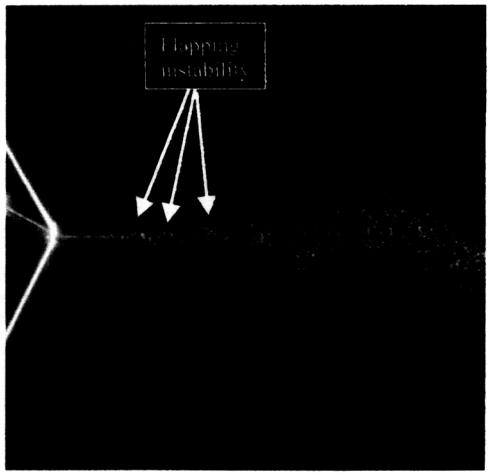

Figure 6: Sample PIV image, Vj = 720 ft/s.

Even though some caution must be exercised in drawing conclusions from these images, there are some general characteristics of the jet that can be observed. First of all, there is definitely a laminar-like region of the jet very near the jet exit. This seems to occur for all velocities tested. There is very little spreading of the jet in this region. As the jet progresses large flapping instabilities are seen in the images. This can actually be seen in at least one image presented for each velocity. This flapping developed with distance and eventually caused the jet to burst suddenly. In some cases the flapping was so strong it could be seen in the burst region as well, and even was extracted by the velocity vector extraction software. Figure 6 shows an image of this flapping in the burst region, and figure 7 shows the velocity vectors extracted by the computer where the flapping tendency of the jet can be seen quite clearly.

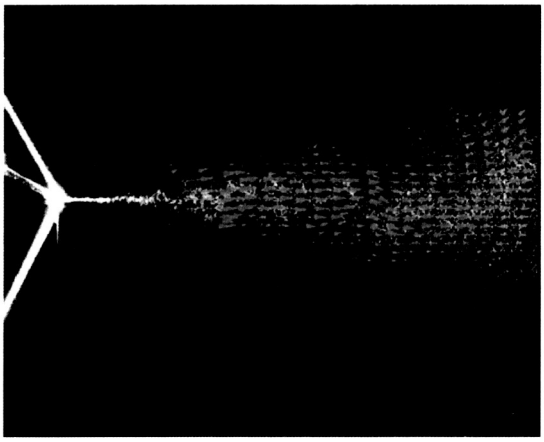

Figure 7: Sample PIV image with velocity vectors.

The flow visualization indicated that the jet has two definite regions of flow. It was desired to determine if in fact the jet was initially laminar at the exit. However, from basic jet flow literature, and in discussions with colleagues working in the field, there does not appear to be a concrete definition of a 'laminar' jet since all jets eventually become turbulent. In general it is assumed that extremely low Reynolds number jets (Re < 30) are defined to be laminar. However, all conditions presented here would be considered turbulent (Re ~ 7,000 – 25,000 for PIV measurements). Perhaps the bursting is simply the transition mixing discussed by Dimotokis.[11] Schlichting[12] also notes that turbulent jets (2-d) have different spreading rates (laminar ~ $x^{2/3}$ and turbulent ~ x) however this trend cannot be ascertained from the PIV data. Pai[13] defines a low-speed laminar jet as one that has mixing only due to molecular transfer. It is probable that this was not the case, at least in the shear layers of the HARN jet. However, the PIV cannot definitively answer that question. Once the bursting occurred, the jet-spread angle was approximately 7°, which is similar to that for round jets. Thus, beyond the burst region, the jet seemed to behave like any other turbulent jet.

In general, the HARN does exhibit many of the typical jet characteristics. The question of whether or not it is initially laminar or turbulent will have to wait until the discussion of the hot-wire data where hopefully more detailed tests will help clear up this issue. In any case, this was kept in mind when taking additional detailed hot-wire measurements. Since there was a good likelihood of the length-scales of these two regions of flow having somewhat independent length-scales, two sets of hot-wire data were typically taken. One set was acquired where the data points were almost assuredly in the pre-burst area of the jet, and one set where the data points were in the post-burst region of the jet.

Hot-wire Measurements

Hot-wire Experimental Set-up

The hot-wire system used was a Dantec Streamline constant temperature anemometer (CTA), model 90N10 frame and 90C10 modules. The system also has a calibration module. The software provided with the system controls the wire set-up, bridge balance, and also contains an automated calibration option, as well as real time average velocity or time signal acquisition. Due to the need for extremely high sampling rates, a separate computer and software system were used to sample and store the hot-wire signal. An HP spectra analyzer that sampled all channels simultaneously at frequencies up to 262 kHz was used to acquire the hot-wire data. This provided plenty of resolution for investigating the turbulence frequencies up to 100 kHz. The data was post-processed using Matlab® software. In-house script files were written to output a mean velocity and turbulence intensity as well as power spectral densities, cross correlations, cross powers, and coherence for the two-wire data. More details of the hot-wire data acquisition can be found in reference [1].

In order to acquire the data, one hot-wire was needed for the profile and turbulence measurements, while two were needed to acquire cross-correlation data. One of the wires in the correlation tests would need to traverse while the other remained stationary. The single wire would also need to traverse. Thus, one wire was mounted by a bar fixed to the HARN stiffening beam, while the other wire was mounted on a two axes traverse, also fixed to the HARN stiffening beam. The hot-wire mounting set-up is shown in figure 8 (a and b). For the single wire measurements, the stationary wire was simply removed from its position.

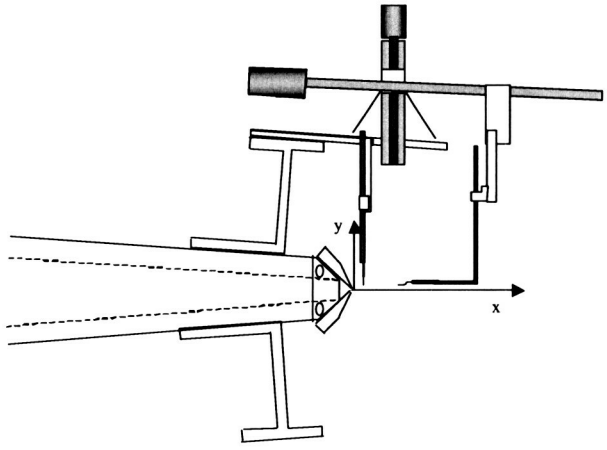

(a)

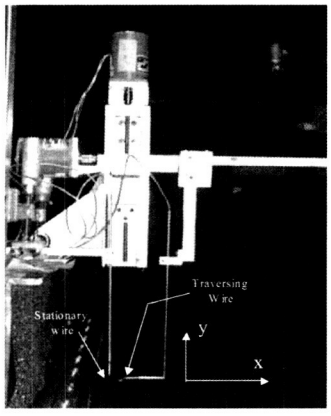

(b)

Figure 8: Hot-wire measurement set-up.

The traversing wire was capable of traversing in the x and y directions independently. One important factor for the traverse system was that it be capable of very minute movements. This was important because the size of the jet emanating from the nozzle was very small, and accurate distances are crucial to properly calculating shear values, length and time scales, as well as the convection velocity.

For the x direction (see figure 8), the minimum traverse movement was 0.000125", while it was 0.0001965" for the y direction. More details of the traverse system and an error analysis of the hot-wire movement is contained in reference [1].

The hot-wires and probe-supports were also obtained from Dantec Measurement Technologies. Two different probe-supports were used, one completely straight (model H21), while the other had a 90° bend (model H22). These are pictured in figure 9a (and are shown installed in position in figure 8). The hot-wires were platinum-plated tungsten 5 μm diameter wires, 1.25 mm long. Several different wire configurations were used for various measurements. The wires used are shown in figure 9b.

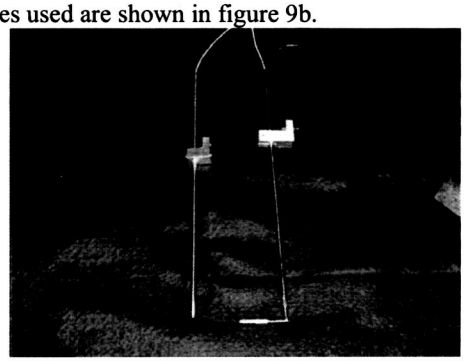

(a)

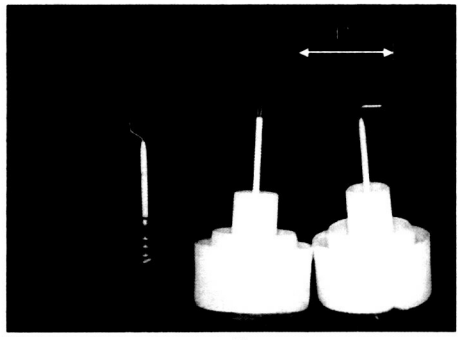

(b)

Figure 9: Hot-wire systems used in measurements. (a) probes, (b) wires.

The HARN was installed on GTRI's Jet Thrust Rig (JTR) for the hot-wire tests. The JTR consists of a small plenum chamber with supply air entering in on one side and a flange on the other side for mounting nozzles. The plenum is mounted to a structure fitted with load cells for thrust measurements. For the hot-wire tests on the HARN, there was no need for thrust measurements, but the facility was available and provided an air supply for the HARN. Reference [1] contains more information on the JTR and the HARN hot-wire set-up.

There was one disadvantage to using the JTR. The JTR is not an acoustic facility and therefore has no provisions for upstream noise reduction. It was feared that internal noise might become significant if there were large mass flows through the upstream piping. This would result from exit conditions that required high mass flows, either due to a large exit area or a high exit velocity. Since the acoustic data in the accompanying study[1,2] were acquired with low upstream noise, it was decided to take most of the hot-wire data at a nozzle width of 6.5" to keep the mass flow and thus any internal noise at a minimum. Basic mean flow and turbulence measurements were taken at

3 velocities. The two-wire data was mostly acquired for only one jet velocity, concentrating on the changes found when varying the slot height. In addition to keeping the internal noise low, lower exit velocities were used to help prolong hot-wire life. During the single wire tests it was found that hot-wires had a significantly shorter life in jets with exit velocities above about 600 ft/s. Thus, during the very time consuming two-wire measurements lower velocities were generally used to minimize wire breakage.

Single Hot-Wire Measurements

The main purpose of the single hot-wire measurements was to gather general information about the HARN jet flow development and compare the findings to lower aspect-ratio jet data available in literature, as well as to round jet data. These measurements mainly consisted of velocity profiles at various downstream locations, centerline velocity traces, and in some cases turbulence intensity information.

Figure 10 shows velocity profiles at several different streamwise locations. As one might expect, the flow very near the exit is nearly plug flow, and the shear layer grows as the profiles are taken father downstream. The profiles can be non-dimensionalized by simply plotting y/h versus V/V_{max}, shown in figure 11. Again the flow starts off like a plug flow, but quickly develops into a self-similar flow. These profiles are compared with data from Schlicting[12] in the figure. Notice that the profiles are very similar to the curves from Schlicting. Different velocities are compared at the same streamwise location in figure 12. These again show that the jet is self-similar beyond the core region of the jet.

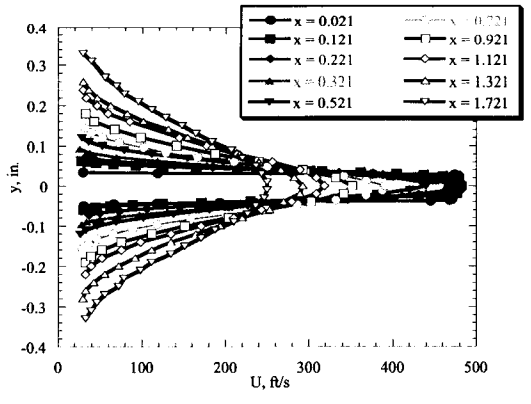

Figure 10: Hot-wire velocity profiles at several downstream locations,

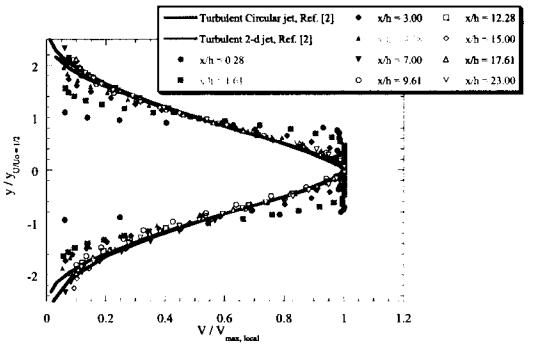

Figure 11: Non-dimensionalized velocity profiles compared with theory,

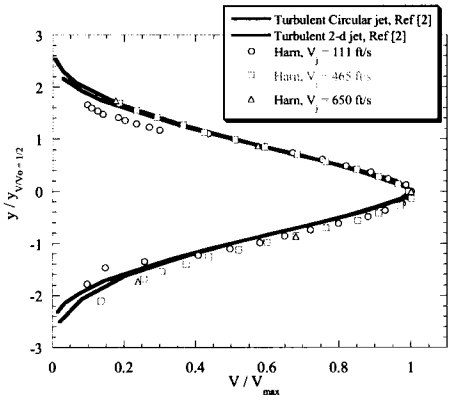

Figure 12: Hot-wire velocity profiles at the same streamwise location for different jet velocities, x/h = 37 (h = 0.040").

Turbulence intensities can also be compared for the different velocities and different locations as shown in figure 13. Near the exit, the turbulence is very low in the core, while very high in the shear layers. As one would expect, the shear layers grow and begin to merge as they progress downstream. None of the previous results were unexpected, however they do confirm that the jet is clean and behaves like a 'normal' jet, i.e., there are no obvious flow differences particular to this nozzle that might explain the different acoustic results found in references [1 and 2].

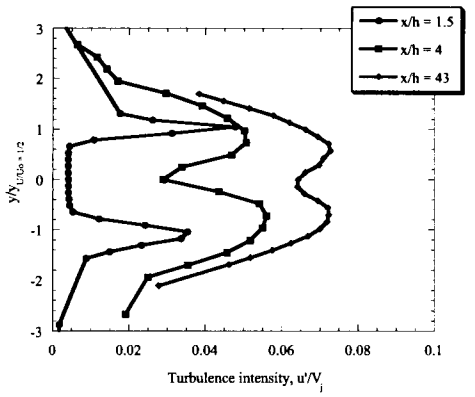

Figure 13: Turbulence intensity at different streamwise locations,

Velocity data were also acquired along the centerline of the jet. Due to the small size of the jet, considerable care had to be taken to verify that indeed the data were taken along the jet centerline. Figure 14 shows the centerline jet velocity for different slot heights. Notice that when velocity is normalized by the jet velocity and axial distance, x, is normalized by the slot height, h, the centerline velocity collapses for different slot heights over a wide range of x/h. Similarly, in figure 15 the centerline velocity is compared at a variety of exit jet conditions. It is worth noting that the core length appears to vary with V_j. There was some concern that increased internal noise of the facility where these measurements were made may have changed the mixing characteristics of the flow through acoustic excitation.[15-17]

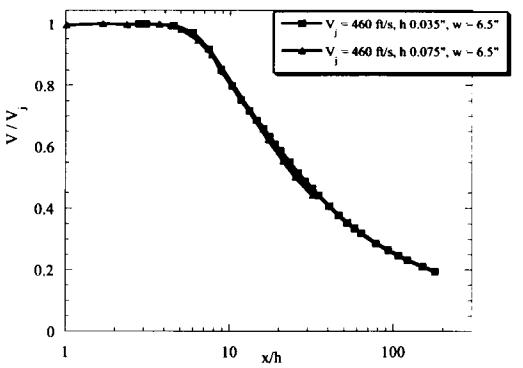

Figure 14: Centerline velocity as a function of x/h for different h.

The experiments were repeated with a muffler mounted between the flow valve and the plenum. As shown in figure 15, similar trends were obtained even with this configuration where the internal noise was reduced considerably. However, this trend has been seen by other researchers also. For example, figure 16 is data taken from Simonich.[18] Simonich noted the relationship between the jet core length and the exit Mach number. He defined the core length as the location where the velocity dropped below 99.5% of the exit velocity.[18] The current data has been plotted on top of the Simonich's data. It should be noted that the figure in reference [18] included data from several researchers, however, here all the data from the paper is shown as the same symbol to distinguish it from the present data. The HARN data falls in the middle of the previous data with a similar trend. This indicates that the change in core length may be a function of the Mach number rather than upstream noise or facility related, since even the data with a muffler installed on the JTR exhibits the same Mach number trend. There is some scatter in the core locations. This may be due to measurement errors associated with small x distances (see reference [1] for a detailed error analysis).

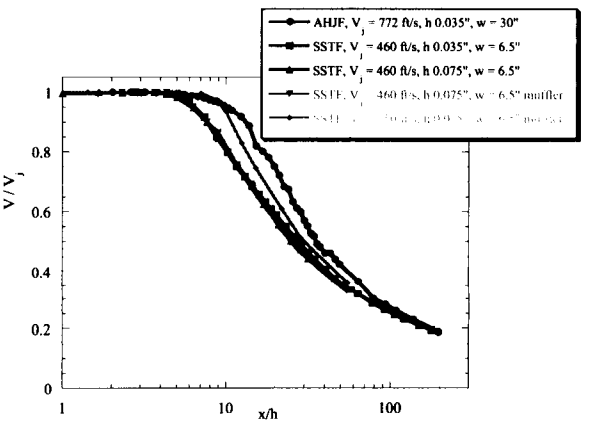

Figure 15: Centerline velocity as a function of x/h for different h, w, and Vj.

Another interesting point to note in figure 15 is the rate of decay of V/V_j with x/h. Typically, for round jets, the rate of decay of the jet velocity is proportional to x/d. Here this decay rate is proportional to $(x/h)^{1/2}$ as illustrated in figure 17. Two of the curves from figure 15 have been re-plotted with a theoretical $(x/h)^{-1/2}$ curve. All of the centerline velocity data was found to be similar to $(x/h)^{-1/2}$ beyond the core. This is similar to the theoretical rate of decrease for a 2-d turbulent jet of $x^{-1/2}$ presented in reference [12]. It should also be noted

that the rate of centerline velocity decrease is $x^{1/3}$ for a 2-d laminar jet.[12] Thus, certainly downstream of the core the jet is definitely turbulent.

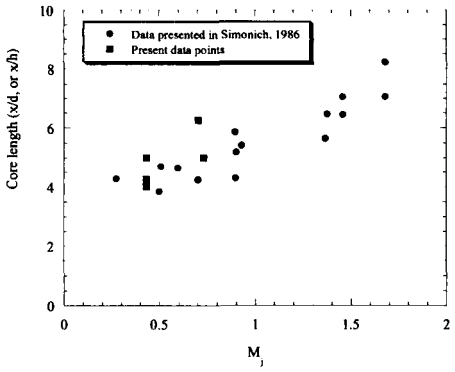

Figure 16: Variation of jet core length as a function of Mach number. Note: circles are data from reference [5], re-plotted.

Another important parameter used to evaluate jets is the spread rate. The jet half-width is commonly defined as the distance from the center of the jet to the location where the velocity is half of the centerline velocity. Using the velocity profile information, the jet half-width was found at each x location for each test condition. These data are plotted in figure 18 with a sample PIV image and the turbulence intensity along the centerline and lip line. Notice that the jet half-width data tends to have a distinct 'knee' where the spread rate (the slope of the half-width vs. x/h curve) drastically changes. This seems to coincide with the 'bursting' of the jet seen in the PIV image around x/h ~ 12. In addition, this generally coincides with higher turbulence intensities.

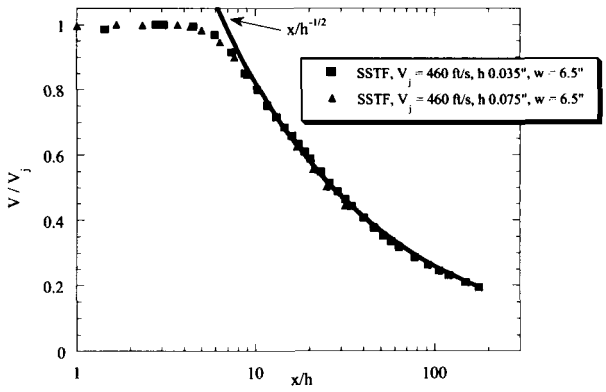

Figure 17: Centerline velocity of HARN compared to theoretical velocity variation.

As mentioned in the discussion of the PIV images, the bursting seems to come from the large instability wave that can be seen in the images just ahead of the burst region. It is not necessarily reasonable to assume that this burst region is self-similar to different slot heights and jet velocities. The instability growth and subsequent burst could be Reynolds number dependent as well as dependent on the upstream noise and turbulence. However, figure 18 indicates that indeed the bursting phenomena of the jet is self-similar since the non-dimensionalized jet half-width and the turbulence intensity tend to collapse for different jet conditions and nozzle geometries.

The single-wire data gave confidence in the hot-wire data acquisition methods. It appeared that the jet was behaving similar to other jets. This provided a background for acquiring the two-wire data in the shear layer of the jet. This initial data also supported the PIV result that there were two distinct regions associated with the flow, one before the burst region, and one after. Thus, the single wire data was a guide for determining where to position the two wires such that length-scales in both regions could be measured.

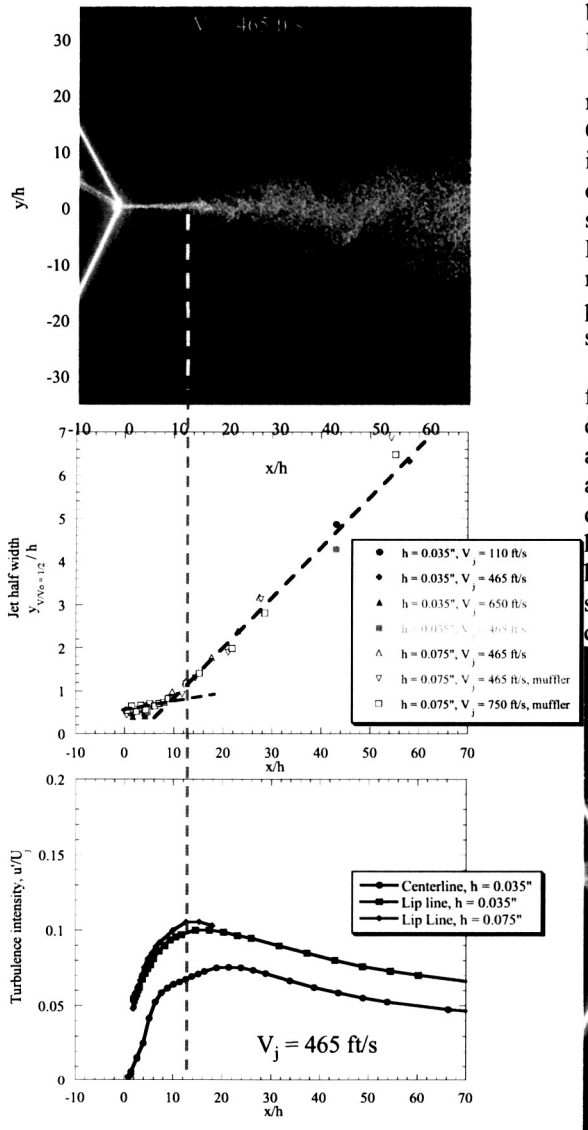

Figure 18: Comparison of PIV, jet half-width, and turbulence intensity results.

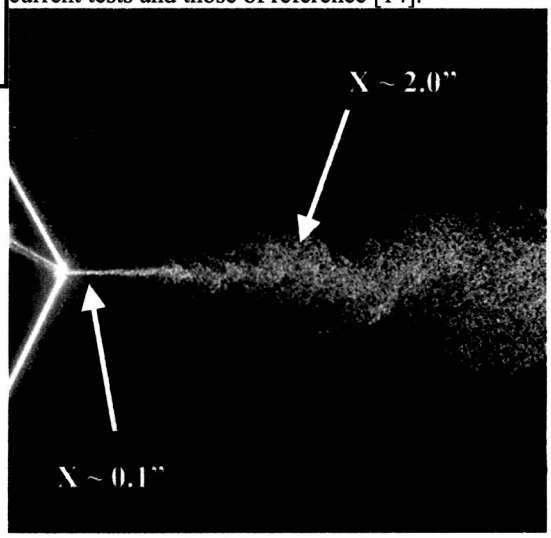

Figure 19: Jet location for cross-correlation data.

Space-Time Correlations with Two-Wire Measurements

As mentioned above, the goal of the two-wire measurements was to determine the length-scales of the HARN jet and to try to relate those length-scales back to the geometry of the nozzle. Davies, Fisher and Barratt[14] performed a study where they made careful hot-wire measurements to find length and time scales for a 1 inch diameter round jet. Using the cross-correlation of the hot-wire time signals, they found integral length and time scales. Their methodology will be followed to calculate similar integral scales for the HARN jet.

Davies, Fisher, Barratt made two-wire measurements primarily at two streamwise locations. One wire was stationary, while the other was traversed in the x or y direction starting from directly behind or directly below the stationary wire. Figure 8 shows the set-up for similar two-wire correlation tests on the HARN. Data were recorded for both wires after moving the traversing wire by some increment. This provided a set of test points where there were two time signals to be analyzed.

Figure 19 shows a schematic of the test points for the HARN jet. Essentially two x locations were chosen, one close to the nozzle exit that would almost assuredly be upstream of the burst region, and one about 2" downstream of the nozzle exit, that was well downstream of the burst region. In order to find out how the scales of the flow varied with changes in slot height, both measurements were repeated for a second slot height. There are some differences between the current tests and those of reference [14]. The most significant is simply a matter of the different nozzle geometries. In the case of reference [14], several radial positions were used for streamwise correlation data, however the nozzle lip-line was where most of their data were acquired and all the data was taken in the shear layer region between the core of the jet and ambient fluid (x/d = 1.5 and x/d = 4.5). Thus, the lip line was always in the region of highest mixing. In the case of the HARN, the measurement location near the nozzle exit was along the lip-line, however the downstream measurement location was well downstream of the core region. Thus, it was decided to place the downstream point at the y location that

corresponded to the jet half-width. This was done because the lip-line at that downstream location would have been considered nearly the center of the jet, since the jet is extremely large compared with the nozzle at high x/h.

At each streamwise location where data were acquired, the two wires were initially positioned as close together as possible, then the traversing hot-wire was traversed downstream, directly behind the stationary wire, or in the case of the y direction, directly below the stationary wire. Figure 20 shows some pictures of the initial wire positions. Precise initial positioning of the wire turned out to be one of the most difficult tasks of this portion of the HARN study. The initial distance between the wires (Δx_o) for a data set was measured visually. If the initial position was accurate, the following measurement points would also have accurate positions since the traverse had very fine movement capability ($\Delta x_{total} = \Delta x_o + \Delta x_{trav}$). However, if the initial position between the two wires was inaccurate, the distance between the two wires is inaccurate until the distance between the wires was such that $\Delta x_o << \Delta x_{trav}$. Very small errors in measuring the distances between the wires made large differences in the post-processing calculations, thus Δx_o was an extremely important measurement. Careful measurement of the initial positions of the wires using the photos seemed to be the best method for determining their positions. They were also aligned in the y-direction in the flow by matching the measured velocity on both wires. This worked well since the velocity changed rapidly with small changes in the y-direction.

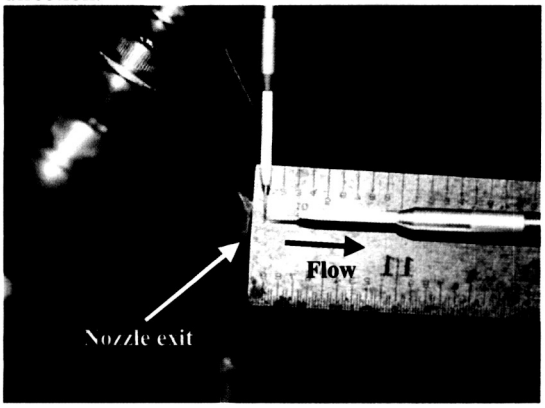

Figure 20: Sample photo of hot-wire placement.

Once the raw hot-wire time histories were taken, they were fed into Matlab where the cross-correlation, the coherence, and the cross-power between the stationary and traversing hot-wire signals were calculated. When Davies, Fisher, and Barratt wrote their paper in 1963, the available computing power was insufficient to perform cross-power spectra and coherence functions on the data, and hence most of their calculations were done using time-domain data. With the impressive capacity of the modern computers, length-scales and time-scales of the HARN flow as a function of frequency in addition to the global values from the cross-correlation can be generated. Most of the HARN data were acquired for a jet velocity of about 465 ft/s. The velocity coincided with the velocity range in reference [14] and was also one of the test points for acoustic data in the accompanying acoustic study in references [1 and 2]. However, this was also a reasonable test point because it was found that the hot-wires broke after much less use at the higher velocities. The slower velocity was also desirable because of the low internal flow rates. Increasing the exit velocity increased the internal velocities, and hence, the internal noise in the test facility used for these measurements. This was a concern since it has been shown that the flow can be excited by internal noise.[15-17] Since internal noise was known to be low for the acoustic tests in references [1 and 2], low internal noise was needed here to maintain the same flow for the hot-wire measurements.

Data were obtained for two slot heights, h ~ 0.035" and h ~ 0.075". As expected, the two hot-wire signals became uncorrelated very quickly at the location near the nozzle. This is due to the much smaller shear layer near the nozzle and therefore the resulting structures will be smaller and dissipate more quickly. However, the downstream location has highly correlated signals over a large separation distance. Since it is much easier to directly compare these data to that of reference [14], the data for the 0.075" height at x = 2.05" (x/h ~ 28) will be used to demonstrate the processing methods.

As already mentioned, there is a great wealth of information that can be extracted from the hot-wire time signals. For all the analysis shown below, the data were recorded at 262 kHz for 14.8 seconds (the maximum that could be stored on the HP analyzer system at one time). This provided ample frequency resolution up to at least 80 kHz for the frequency domain analysis, and the 14.8 seconds provided enough time for over 200 averages when taking the FFT, the coherence, and the cross-power spectra. For more details on the processing of the data, the reader is referred to reference [1].

The space correlation coefficient is defined as the cross-correlation of the time signals in space and is

$$R_x = \frac{1}{T}\int_0^T \frac{\overline{v_1(0)v_2(x)}}{\overline{v_1^2}}dt, \qquad (1)$$

noting that R_x is the correlation coefficient in the x direction and v_1 and v_2 are the fluctuating velocity

signals from the respective hot-wires. The integral length-scale is defined[14] as follows:

$$L_x = \int_0^\infty R_x dx. \quad (2)$$

This is related to the longitudinal integral scale of the turbulence[14]. By introducing a time shift, τ, to one of the signals, the cross-correlation can be calculated as

$$R_{x\tau} = \frac{1}{T}\int_0^T \frac{\overline{v_1(0,0)v_2(x,\tau)}}{\overline{v_1^2}} dt, \quad (3)$$

noting that $R_{x\tau}$ is a function of both x and τ. Plotting $R_{x\tau}$ versus τ allows for several observations. Each pair of signals at a given Δx between the wires produces an $R_{x\tau}$ versus τ curve. Note from the equation for $R_{x\tau}$ that the value of $R_{x\tau}$ for $\tau = 0$ is the value of R_x for that particular set of signals. Davies, Fisher and Barratt also stated that the peak of each curve represents the convection of energy-bearing turbulent eddies, and that the curve produced by taking the peak point of each curve is the auto-correlation of the energy-containing eddies of the flow in a moving frame traveling at the convection velocity.[14] The integral of this curve is referred to as the moving-axis integral time-scale, defined as

$$L_\tau = \int_0^\infty R_{\tau c} d\tau. \quad (4)$$

This is the rate at which the turbulence changes with time.

Convection velocities can be calculated from the resulting scales, $V_c \sim L_x/L_\tau$. Alternatively, by noting the time of each cross-correlation peak and the Δx between the wires, convection velocity for these eddies can be calculated.

The following figures and discussion will follow the methodology of reference [14], and will show the progression of the data processing for one example. Once the process has been shown using the sample data set, the resultant length scales, plus the convection velocities for all the test cases will be presented. For each data set the initial traverse increment for the hot-wire was very small to guarantee a high correlation between the signals at least for a few points. Eventually the increment between data points was increased so that the entire correlation length could be covered with a reasonable number of points. Figure 21 shows a sample distribution of data points in the x-direction. Figure 22 is the cross-correlation of the data, $R_{x\tau}$. Keep in mind that each curve represents one set of time history files. In this particular figure, only the data for every other Δx point is plotted to reduce the clutter on the plot for demonstration purposes. Figure 23 shows only a few of the curves from figure 22 and graphically demonstrates how R_x, and R_τ are pulled from the cross-correlation data. Figure 24 is the plot of R_x, corresponding to the data in figure 22b. This curve can be integrated numerically, resulting in L_x = 0.15" for this case.

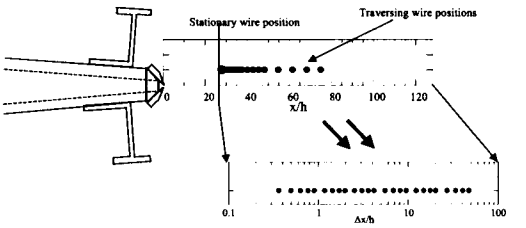

Figure 21: Distribution of data points for correlation data.

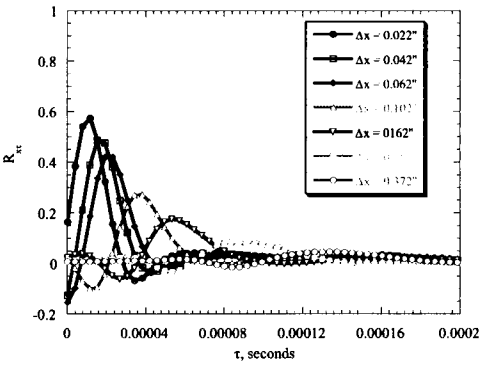

(a)

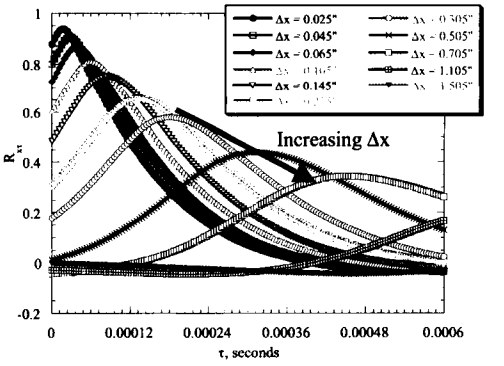

(b)

Figure 22: Cross-correlation of two hot-wires at several Dx, h ~ 0.075", Vj = 465 ft/s. (a) xstationary = 0.10", (b) xstationary = 2.10"

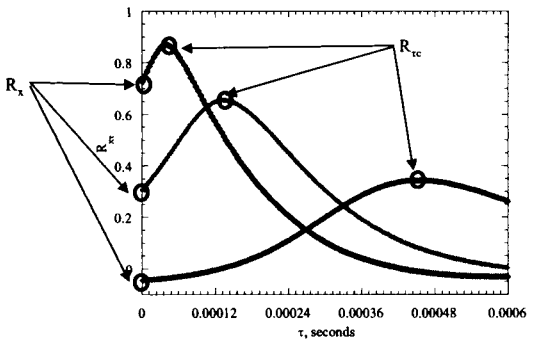

Figure 23: Illustration of how the space-correlation and auto-correlation of the energy containing eddies are found from the cross-correlation.

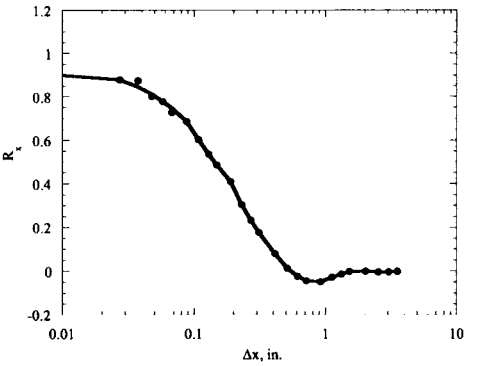

Figure 24: Space-correlation for the data in figure 24(b).

Following this process for all the data sets, the length-scale can be plotted for each condition. The length-scales are plotted versus x location in figure 25. There are only a few points to examine, but it is still worthwhile to find a relationship between the points. In reference [14] a linear relationship between L_x and x was found for the round jet. In the present study, there does not appear to be a linear relationship between L_x and x or L_x/h and x/h. After examining several different possible relationships, it was found that the $L_x \sim x(AR)^{1/4}$. This is shown in figure 26 where the x location is multiplied by the aspect-ratio factor. This is a rather unusual relationship and hence requires some closer examination.

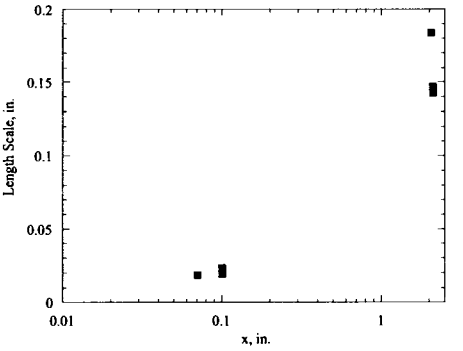

Figure 25: Global length scales calculated from the space-correlation in figure 20.

Based on relationship found in figure 26 some rather interesting observations can be made. By substituting w/h for aspect ratio and multiplying by h/h, the following re-organization can be done:

$$L_x \sim x(AR)^{1/4} \quad (5)$$

$$L_x \sim x\left(\frac{w}{h}\right)^{1/4} \quad (6)$$

$$L_x \sim x\frac{h}{h}\left(\frac{w}{h}\right)^{1/4} \sim \frac{x}{h}h^{3/4}w^{1/4} \sim \frac{x}{h}L_{eq}, \quad (7)$$

Thus, it appears the length-scale is proportional to the streamwise location and the equivalent length $L_{eq} = h^{3/4}w^{1/4}$ if the manipulation is appropriate. This is the same scale that was found to scale the acoustic spectra in references [1 and 2].

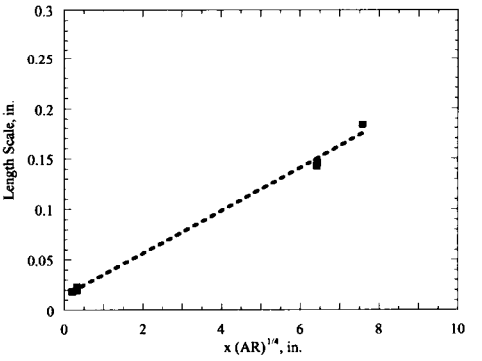

Figure 26: Global length scales plotted as a linear function of location and aspect-ratio.

It is generally accepted that different frequencies are radiated from different locations in the

jet.[18] Typically, high frequency noise is generated very near the nozzle while low frequency noise is generated at some distance from the nozzle exit. Thus, it can be assumed that the majority of noise generated for a particular frequency is generated at a particular streamwise location, x/h. It therefore makes sense that Lx ~ x/h and is reasonable to extract an x/h from the relationship. Once this is done, the equivalent length falls out of the relationship. Therefore, the length-scale for a given frequency is directly proportional to L_{eq}. This is an extremely important result in that it supports the scaling parameters identified in the acoustic study on the same nozzle.[1, 2] However, it must be admitted that this result was extracted from a very few number of data points, and also that w was constant for all these tests. However, the fact that the equivalent-length defined during the acoustic data analysis can be derived as the appropriate length-scale for the flow from hot-wire data is noteworthy. The reader is cautioned that this result needs more examination. However, due to time constraints and facility schedule a more detailed investigation of this will have to be left to future work. It will suffice here to state that the length-scales responsible for generating a particular frequency of noise appears to be proportional to $h^{3/4}w^{1/4}$ which was also borne out by the HARN acoustic data for the same configurations.[1, 2]

Variation of Convection Velocity with Frequency

Another parameter important to the aeroacoustics of the HARN that can be extracted from the two-wire measurements is the convection velocity of the turbulent eddies. Convection velocity can be calculated from the information already discussed. If one again returns to figure 22 of the cross correlation of the time signals, it was noted that for each wire spacing there is a cross-correlation curve. The peak of the cross-correlation curve is associated with time it takes the convected eddies to move from the first wire to the second wire. Since the distance between the wires is known, a convection speed can be calculated. A velocity can be calculated for each spacing, producing convection speed as a function of x (wire location). Normally it is assumed that the convection speed is approximately 0.65 V_j. Figure 27 is a plot of the convection velocity normalized by the jet exit velocity for several data-sets. Notice that this does not correlate with the assumed value of 0.65 for the ratio V_c/V_j. However, notice that near the exit of the nozzle (x/h < 5) the ratio of velocities is near 0.6. Clearly the jet exit velocity is not the proper scale for the convection velocity throughout the jet.

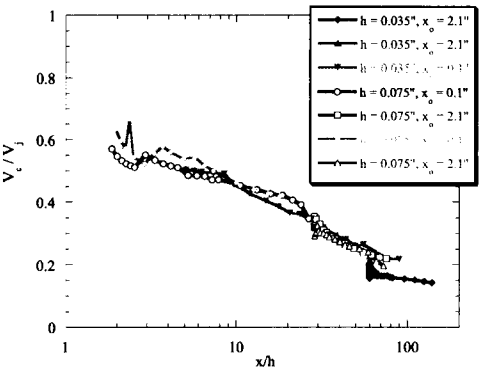

Figure 27: Convection velocity normalized by jet exit velocity.

The convection velocity drops as the local velocity drops with increasing x/h. Figure 28 is the same data normalized by the local centerline jet velocity, V_t. Notice that this ratio varies from 0.50 – 0.80, with an average value of 0.65. This is an important result since much of the work using a convection speed, or convection Mach number, simply uses 0.65 of the exit Velocity or Mach number. This is not strictly correct as shown in the previous figures. In fact, if one number is used to represent the convection velocity, it should be less than 0.65 V_j since $V_c \sim 0.65\ V_t$ and $V_t < V_j$ (except near the core).

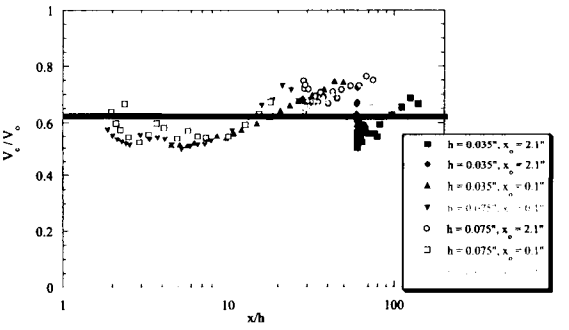

Figure 28: Convection velocity normalized by the jet centerline velocity at the appropriate x/h.

In addition to the variation of the convection speed with distance from the nozzle exit, some researchers have shown a variation of convection velocity with the frequency, or wavelength, of the eddy being convected. For example, De Belleval et al.,[20] showed this type of result, but gave no discussion on the topic, merely noting that the average was 0.65 V_j.

Only global convection speed can be calculated using the method in reference [14]. However, the capability now exists where the hot-wire data can easily be converted into the frequency domain, and the convection speed can be calculated for each frequency using the cross-power between the two signals. Since the cross-power is generally a complex number, it is appropriate to separate it into a magnitude and phase. The magnitude is a relative estimate of how correlated the signals are, while the phase is the relative phase between the two signals.

Figure 29 (a and b) is an example of the cross-spectra between the two wires for several values of Δx. Notice that the magnitude of the cross-power decreases as Δx increases, particularly at frequencies greater than 500 Hz. The phase also seems to indicate that less of the spectrum is correlated as the wires separation grows. This is shown by the phase curves' smooth portion at low frequencies that eventually progresses into a random varying region as frequency is increased.